Journal of The Electrochemical Society, 2023 **170** 030510

On the Error of Li-ion Battery Parameter Estimation Subject to System Uncertainties

Jackson Fogelquist,[1] Qingzhi Lai,[1] and Xinfan Lin[1,z]

Department of Mechanical and Aerospace Engineering, University of California, Davis, California 95616, United States of America

Emerging lithium-ion battery systems require high-fidelity electrochemical models for advanced control, diagnostics, and design. Accordingly, battery parameter estimation is an active research domain where novel algorithms are being developed to calibrate complex models from input-output data. Amidst these efforts, little focus has been placed on the fundamental mechanisms governing estimation accuracy, spurring the question, why is an estimate accurate or inaccurate? In response, we derive a generalized estimation error equation under the commonly adopted least-squares objective function, which reveals that the error can be represented as a combination of system uncertainties (i.e., in model, measurement, and parameter) and uncertainty-propagating sensitivity structures in the data. We then relate the error equation to conventional error analysis criteria, such as the Fisher information matrix, Cramér-Rao bound, and parameter sensitivity, to assess the benefits and limitations of each. The error equation is validated through several uni- and bivariate estimations of lithium-ion battery electrochemical parameters using experimental data. These results are also analyzed with the error equation to study the error compositions and parameter identifiability under different data. Finally, we show that adding target parameters to the estimation without increasing the amount of data intrinsically reduces the robustness of the results to system uncertainties.

 [DOI: 10.1149/1945-7111/acbc9c]

Manuscript submitted November 9, 2022; revised manuscript received January 21, 2023. Published March 9, 2023.

Data-based parameter estimation can be generally defined as fitting a mathematical model to data through the identification of numerical constants. Accordingly, it is a vital element of model-based control, which strongly relies upon accurate models of physical systems. Recently, the accelerating deployment of electric vehicles and renewable energy systems has spurred significant research interest in the estimation of electrochemical parameters for lithium-ion (Li-ion) batteries,[1–3] which enables the high-fidelity battery modeling capabilities necessary for advanced battery management systems,[4] fast-charging control,[5] and degradation monitoring.[6]

There are three fundamental elements of a parameter estimation problem: measurement data, system model, and estimation algorithm. The algorithm is a set of optimization procedures for determining the values of model parameters that minimize a cost function associated with the error between the measurement data and model predictions, e.g., sum of squared errors. As such, several challenges exist that negatively affect the estimation performance. For example, nonlinear models and large parameter sets can cause identifiability issues and high computational expense.[3,7] More notably, the measured data may not contain sufficient information about the target parameters, which can limit the attainable estimation accuracy,[8] e.g., a given parameter may be accurately estimated under one data set but become unidentifiable under another.

Accordingly, efforts have been made to study the quality of data and its influence on the estimation result. In the field of battery modeling and control, existing analysis methods are mostly based on parameter sensitivities, the Fisher information, and the Cramér-Rao bound. Sensitivity analysis examines the relationship between the system output data and parameter values, and can be classified as either local or global. Local sensitivity analysis quantifies the sensitivity of the system output to a given parameter under a fixed assumed/nominal parameter set (i.e., at a point in the parameter space), whereas global analysis examines the parameter sensitivity by evaluating the output under different combinations of parameter values (i.e., across the entire parameter space).[9] For example, Refs. 10, 11 examined the sensitivity dynamics of electrochemical battery parameters through analytical local sensitivity analyses; Refs. 2, 12 ranked the sensitivities of electrochemical battery parameters through numerical local sensitivity analyses; and Refs. 13, 14 used global sensitivity analyses to compare sensitivities among different battery parameters and study their interactions (i.e., the influence of simultaneously changing combinations of parameters on the output). Computed based on parameter sensitivities, the Fisher information can be used to quantify the amount of information about the parameters that is embedded in the data.[15] In Ref. 16, the eigenvalues of the Fisher information matrix were used to rank the identifiability of electrochemical battery parameters. The Fisher information matrix was analytically derived in Ref. 17 to examine the identifiability of a simple battery model under periodic excitation. Furthermore, the inverse of the Fisher information gives the Cramér-Rao bound, which characterizes the lower bound of the estimation error (co)variance for an unbiased estimator.[15,18] In Refs. 19–21, the Cramér-Rao bound was analytically derived for uni- and multivariate state and parameter estimation for an equivalent circuit battery model under generic excitation, to quantify the role of battery characteristics and data on estimation accuracy. Additionally, since the Cramér-Rao bound indicates that error (co)variance is minimized when the Fisher information is maximized (under certain metrics), scalar Fisher information-based criteria (e.g., determinant, trace, minimum eigenvalue) have become standard metrics for data quality and are typically implemented in optimal experiment design to improve the parameter estimation accuracy.[22–24] Numerous other analysis criteria have also been applied to battery estimation problems, including entropy-based criteria[25,26] and confidence interval analysis.[27,28]

These existing estimation accuracy analyses have limitations because they do not consider estimation bias nor system uncertainties. The effectiveness of these analyses is thus significantly restricted, as estimation bias and system uncertainties are major sources of estimation error and are inevitable in practice.[8] Specifically, estimation accuracy has been shown to be strongly influenced by constant and varying uncertainty in model (e.g., due to unmodeled dynamics),[29] measurement (e.g., due to sensor bias/noise),[30] and (non-estimated) parameters (e.g., due to changing operating conditions/degradation).[31] We sought to address these limitations in a prior work through the derivation of a univariate estimation error equation for the least-squares objective, which directly predicts the estimation error through consideration of

[z]E-mail: lxflin@ucdavis.edu

uncertainties in model, measurement, and parameter.[8] This error equation was subsequently leveraged to develop criteria for data optimization in univariate estimation scenarios, i.e., cost functions for input excitation design[8] and criteria for data selection,[32,33] which yielded promising results and outperformed the conventional Fisher information-based criteria.

The purpose of this paper is to answer the fundamental question —why is an estimation result accurate or inaccurate?—both from a generic perspective and in the context of battery parameter estimation problems. The topic is investigated through the following contributions. First, we will derive and validate a generalized multivariate estimation error equation under the least-squares objective function that is not subject to conventional limitations (i.e., unbiased estimation and omission of system uncertainties). This equation will reveal several important insights, such as the theoretical relationship between system uncertainties and estimation error, data structures that are capable of attenuating (or amplifying) the influence of system uncertainties, and the precedence of data quality over quantity. Second, we will apply this equation to analyze the error composition and parameter identifiability in several battery electrochemical parameter estimation scenarios under various data sets. This will indicate the factors that enhance/degrade estimation accuracy and illustrate their strong dependence on data. Third, we will compare the errors and their compositions across uni- and bivariate estimation scenarios to demonstrate an intrinsic mechanism that can reduce accuracy as additional parameters are simultaneously estimated under the same data. These contributions cast new light on the state of the art estimation error analysis methods. As the traditional criteria do not consider estimation bias nor system uncertainties, we will explicitly reveal how these factors affect the estimation errors. Specifically, traditional local and global sensitivity analyses indicate that the magnitude of parameter sensitivity is important, yet we will show that the structure of sensitivity can have an even greater impact on the estimation result in the presence of uncertainties. Similarly, Fisher information-based criteria specify that estimation performance will always improve with the amount of data, though we will show that the structure of the data plays a more significant role and unfavorable data can potentially degrade the accuracy under uncertainty.

The organization of the remainder of this paper is as follows. First, we present the derivation and analysis of the generalized multivariate estimation error equation. Second, we provide a brief summary of the battery physics and model associated with our application of electrochemical parameter estimation. Third, we apply the estimation error equation to analyze the accuracy of univariate electrochemical parameter estimation under a series of data sets. Fourth, we extend the analysis to the bivariate estimation case, and finally, we present concluding remarks and anticipated avenues of future work.

Derivation & Analysis of Estimation Error

In this section, we will derive and discuss the estimation error equation that will be implemented for error analysis in the proceeding sections. Consider a discrete-time single-input-single-output system model,

$$\begin{aligned} \boldsymbol{x}_k &= \boldsymbol{f}_k(\boldsymbol{x}_{k-1}, \boldsymbol{\theta}, \boldsymbol{\phi}, u_{k-1}) \\ y_k &= g_k(\boldsymbol{x}_k, \boldsymbol{\theta}, \boldsymbol{\phi}, u_k), \end{aligned} \quad [1]$$

which can be used to characterize most battery models, e.g., the commonly implemented equivalent circuit model, as well as the Doyle-Fuller-Newman (DFN) model[34] and single particle model (SPM)[35] after spatial discretization of the partial differential equations (PDEs). In Eq. 1, $\boldsymbol{x}$, u, and y are the state vector, input, and output of the system, $\boldsymbol{f}$ and g are the nonlinear state and output equations, and k is the time step index. The system is parameterized by $\boldsymbol{\theta}$ and $\boldsymbol{\phi}$, where $\boldsymbol{\theta} = [\theta_1,\ldots,\theta_n]^T$ is the vector of target parameters to be estimated and $\boldsymbol{\phi} = [\phi_1,\ldots,\phi_m]^T$ is the vector of non-estimated system parameters.

The objective of the estimation problem is to determine $\boldsymbol{\theta}$ based on a sequence of N measured output data $\boldsymbol{y}^m = [y_1{}^m,\ldots,y_N{}^m]^T$ sampled across consecutive time steps under input sequence $\boldsymbol{u} = [u_1,\ldots,u_N]^T$. To incorporate various system uncertainties, each output measurement $y_k{}^m$ is expressed as

$$y_k^m = y_k(\boldsymbol{\theta}, \boldsymbol{\phi}, \boldsymbol{u}_k) + \Delta y + \delta y_k, \quad [2]$$

where $y_k(\boldsymbol{\theta}, \boldsymbol{\phi}, \boldsymbol{u}_k)$ is the modeled system output under the true parameter values $(\boldsymbol{\theta}, \boldsymbol{\phi})$, Δy is the model/measurement bias, and δy_k is the varying model/measurement uncertainty. The model/measurement uncertainty terms Δy and δy_k characterize the mismatch between the modeled output $y_k(\boldsymbol{\theta}, \boldsymbol{\phi}, \boldsymbol{u}_k)$ and measured output $y_k{}^m$ due to factors such as unmodeled system dynamics, discretization errors, and sensor bias/noise. For example, the battery SPM is derived from the full-order DFN model under the simplifying assumption of uniform reaction current density across each electrode, which results in unmodeled dynamics that degrade model accuracy under a large current amplitude.[11,36] In fact, even the DFN model contains simplifying assumptions that contribute to voltage prediction errors (e.g., electrode particles are spherical with uniform radii), as no model is capable of perfectly representing physical phenomena. Model uncertainty is compounded by distortions in the system input/output measurements caused by sensor bias and noise, which are also incorporated in the terms Δy and δy_k. While model uncertainty may render errors when using the model for prediction, it is still meaningful and important to achieve accurate parameter estimation, particularly when the parameters have physical significance. One example is battery state of health (SOH) monitoring with an electrochemical model, in which health-related physical parameters must be accurately estimated to indicate trends in cell degradation.[27,37,38] Thus, we emphasize the importance of parameter estimation error analysis, especially under scenarios of high model/measurement uncertainty. Finally, in this work, we assume that the initial conditions are known for a given data set, though there could be uncertainty in the initial conditions in practice, which may be considered a form of model uncertainty and thus incorporated in the terms Δy and δy_k. It is noted that $y_k(\boldsymbol{\theta}, \boldsymbol{\phi}, \boldsymbol{u}_k)$ denotes the mapping from $\boldsymbol{\theta}$, $\boldsymbol{\phi}$, and $\boldsymbol{u}_k$ to y_k with the state dynamics contained implicitly, i.e., $\boldsymbol{u}_k \rightarrow G_k(\boldsymbol{\theta}, \boldsymbol{\phi}) \rightarrow y_k$, where $\boldsymbol{u}_k = [u_1,\ldots,u_k]^T$.

In the practice of parameter estimation, the least-squares optimization objective is the most commonly (if not the only) used criterion. Indeed, it is almost universal, as most existing works either use gradient-based methods to solve the least-squares estimation problem in batch[2,16,27] or recursive formulations (e.g., Kalman filter[30,39] and moving horizon observer[40] among others), or employ advanced non-gradient-based methods to optimize the same objective (e.g., the least-squares objective has been solved with the genetic algorithm in Ref. 41, particle swarm optimization algorithm in Ref. 42, and cuckoo search algorithm in Ref. 3). The discrete-time least-squares objective determines the estimated parameter set $\hat{\boldsymbol{\theta}}$ by minimizing the sum of squared errors between the measured output $y_k{}^m$ and modeled output y_k across the N data points,

$$\min_{\hat{\boldsymbol{\theta}}} J = \frac{1}{2}\sum_{k=1}^{N}(y_k^m - y_k(\hat{\boldsymbol{\theta}}, \hat{\boldsymbol{\phi}}, \boldsymbol{u}_k))^2. \quad [3]$$

It is noted that the estimation problem further includes parameter uncertainty in $\boldsymbol{\phi}$, as the exact values may not be known, which is indicated by the notation $\hat{\boldsymbol{\phi}}$ in Eq. 3. In estimation practice, there are usually parameters that are not estimated due to reasons including insignificant impact on system performance, lack of identifiability, or the need to reduce the complexity of the estimation. Therefore, nominal values of these parameters are adopted. In the battery context, uncertainty in these parameters (deviation from the nominal

values) is often caused by manufacturing variation, cell degradation, operating condition, and inaccurate model identification.

To analyze the estimation error under the least-squares objective, we apply the first-order optimality condition ($\nabla_{\hat{\boldsymbol{\theta}}} J = \mathbf{0}$) to Eq. 3, which yields

$$-\sum_{k=1}^{N} \frac{\partial y_k^T}{\partial \hat{\boldsymbol{\theta}}}(\hat{\boldsymbol{\theta}}, \hat{\boldsymbol{\phi}}, \boldsymbol{u}_k)(y_k^m - y_k(\hat{\boldsymbol{\theta}}, \hat{\boldsymbol{\phi}}, \boldsymbol{u}_k)) = \mathbf{0}, \quad [4]$$

where $\frac{\partial y_k}{\partial \hat{\boldsymbol{\theta}}} = \left[\frac{\partial y_k}{\partial \hat{\theta}_1}, \ldots, \frac{\partial y_k}{\partial \hat{\theta}_n}\right]$ is the (row) vector of output sensitivity to each target parameter in $\hat{\boldsymbol{\theta}}$ at time step k, and $\mathbf{0}$ is the n-dimensional null column vector. Recall that the measured output y_k^m is represented in function of the (unknown) true parameter values ($\boldsymbol{\theta}$, $\boldsymbol{\phi}$) in Eq. 2. Therefore, we expand $y_k(\boldsymbol{\theta}, \boldsymbol{\phi}, \boldsymbol{u}_k)$ with a first-order Taylor series about the estimated/assumed parameter values ($\hat{\boldsymbol{\theta}}$, $\hat{\boldsymbol{\phi}}$), i.e.,

$$y_k(\boldsymbol{\theta}, \boldsymbol{\phi}, \boldsymbol{u}_k) \approx y_k(\hat{\boldsymbol{\theta}}, \hat{\boldsymbol{\phi}}, \boldsymbol{u}_k) + \frac{\partial y_k}{\partial \hat{\boldsymbol{\theta}}}(\hat{\boldsymbol{\theta}}, \hat{\boldsymbol{\phi}}, \boldsymbol{u}_k)\Delta\boldsymbol{\theta} + \frac{\partial y_k}{\partial \hat{\boldsymbol{\phi}}}(\hat{\boldsymbol{\theta}}, \hat{\boldsymbol{\phi}}, \boldsymbol{u}_k)\Delta\boldsymbol{\phi}, \quad [5]$$

where $\Delta\boldsymbol{\theta} = \boldsymbol{\theta} - \hat{\boldsymbol{\theta}}$ is the estimation error in $\hat{\boldsymbol{\theta}}$, $\Delta\boldsymbol{\phi} = \boldsymbol{\phi} - \hat{\boldsymbol{\phi}}$ is the parameter uncertainty in $\hat{\boldsymbol{\phi}}$, and $\frac{\partial y_k}{\partial \hat{\boldsymbol{\phi}}} = \left[\frac{\partial y_k}{\partial \hat{\phi}_1}, \ldots, \frac{\partial y_k}{\partial \hat{\phi}_m}\right]$ is the (row) vector of output sensitivity to each non-estimated parameter in $\hat{\boldsymbol{\phi}}$ at time step k.

Combining Eqs. 2, 4, and 5 and rearranging yields the multivariate estimation error equation

$$\Delta\boldsymbol{\theta} = -\left(\sum_{k=1}^{N} \frac{\partial y_k^T}{\partial \hat{\boldsymbol{\theta}}}\frac{\partial y_k}{\partial \hat{\boldsymbol{\theta}}}\right)^{-1}\left[\left(\sum_{k=1}^{N} \frac{\partial y_k^T}{\partial \hat{\boldsymbol{\theta}}}\right)\Delta y + \left(\sum_{k=1}^{N} \frac{\partial y_k^T}{\partial \hat{\boldsymbol{\theta}}}\delta y_k\right) + \left(\sum_{k=1}^{N} \frac{\partial y_k^T}{\partial \hat{\boldsymbol{\theta}}}\frac{\partial y_k}{\partial \hat{\boldsymbol{\phi}}}\right)\Delta\boldsymbol{\phi}\right], \quad [6]$$

which expresses the estimation error $\Delta\boldsymbol{\theta}$ in terms of the parameter sensitivities and system uncertainties, i.e., the model/measurement bias Δy, varying model/measurement uncertainty δy_k, and parameter uncertainty vector $\Delta\boldsymbol{\phi}$. Note that the sensitivities are dependent on $\hat{\boldsymbol{\theta}}$, $\hat{\boldsymbol{\phi}}$, and $\boldsymbol{u}_k$, though these terms are omitted for brevity. If $\hat{\theta}$ and $\hat{\phi}$ are scalars, Eq. 6 is reduced to a more compact scalar form,

$$\Delta\theta = -\frac{\left(\sum_{k=1}^{N} \frac{\partial y_k}{\partial \hat{\theta}}\right)\Delta y + \left(\sum_{k=1}^{N} \frac{\partial y_k}{\partial \hat{\theta}}\delta y_k\right) + \left(\sum_{k=1}^{N} \frac{\partial y_k}{\partial \hat{\theta}}\frac{\partial y_k}{\partial \hat{\phi}}\right)\Delta\phi}{\sum_{k=1}^{N}\left(\frac{\partial y_k}{\partial \hat{\theta}}\right)^2}. \quad [7]$$

Several insights can be drawn from the estimation error equation.

1. Using more data for estimation (i.e., measurements of input/output physical quantities, such as current, voltage, and temperature in a battery system) does not necessarily improve estimation accuracy, when the data contain high levels of uncertainty and are weakly sensitive to the target parameters. We illustrate this by examining the scalar form of the error equation in Eq. 7, which indicates that, while increasing the number of data points (N) will monotonically increase the denominator, the numerator may also increase and possibly at a higher rate. For example, if the sensitivity $\frac{\partial y_k}{\partial \hat{\theta}}$ is small (<1), the approximately linear rate of increase of the numerator could outpace the quadratic rate of the denominator. Alternatively, consider that the varying model/measurement uncertainty δy_k may be very large during a portion of the data. The estimation error could be reduced by using a subset of the data that has high sensitivity or avoids the highly uncertain portion. This insight is corroborated by several works that have improved estimation accuracy through strategic data selection from a larger data set.[32,33,39]
2. The term $\sum_{k=1}^{N} \frac{\partial y_k^T}{\partial \hat{\boldsymbol{\theta}}}\frac{\partial y_k}{\partial \hat{\boldsymbol{\theta}}}$ is essentially the Fisher information matrix simplified under independently and identically distributed (i.i.d.) Gaussian noise.[17,21] Thus, we see that the Fisher information is directly related to the estimation error and serves as an approximate measure of robustness against the influence of system uncertainties. This is more intuitive in the scalar error equation in Eq. 7, where a large Fisher information in the denominator will attenuate the impact of the system uncertainty terms in the numerator. However, the Fisher information is only part of the equation and is thus not a sole indicator of estimation accuracy. For example, Eq. 7 shows that a large error will occur if the uncertainty terms in the numerator are significantly larger than the Fisher information in the denominator, regardless of the size of the Fisher information. The same conclusion can be obtained for the multivariate case by applying norm analysis to the general form in Eq. 6. Therefore, it is critical to consider the role of system uncertainties in estimation error analysis. Additionally, the error equation cannot be computed if the Fisher information matrix is not invertible, which is consistent with the conventional criterion that a system is not uniquely identifiable if the Fisher information matrix is singular.[17,43] Finally, we see that Fisher information-based criteria favor more data for estimation, which may not be optimal according to the previous insight on data length.
3. The term $\left(\sum_{k=1}^{N} \frac{\partial y_k^T}{\partial \hat{\boldsymbol{\theta}}}\right)\Delta y$ represents the error caused by the constant model/measurement uncertainty Δy. It is seen that Δy is propagated to the total error through the sensitivity structure $\sum_{k=1}^{N} \frac{\partial y_k^T}{\partial \hat{\boldsymbol{\theta}}}$. Therefore, the influence of Δy is eliminated if $\sum_{k=1}^{N} \frac{\partial y_k^T}{\partial \hat{\boldsymbol{\theta}}} = \mathbf{0}$, i.e., the sensitivity of (each) target parameter sums to zero across the data sequence. This relationship between a specific sensitivity structure and the estimation error illuminates the limitation of traditional sensitivity analysis methods, which only focus on the magnitude of sensitivity.
4. The term $\sum_{k=1}^{N} \frac{\partial y_k^T}{\partial \hat{\boldsymbol{\theta}}}\delta y_k$ represents the error caused by the varying model/measurement uncertainty δy_k. Essentially, this term is a vector of inner products between the sensitivity sequence vector for each target parameter $\frac{\partial \boldsymbol{y}}{\partial \hat{\theta}_i} = \left[\frac{\partial y_1}{\partial \hat{\theta}_i}, \ldots, \frac{\partial y_N}{\partial \hat{\theta}_i}\right]$ and the uncertainty sequence vector $\delta\boldsymbol{y} = [\delta y_1, \ldots, \delta y_N]^T$, where each vector consists of the respective entries across all time steps of the sequence. Accordingly, the influence of δy_k on the estimation error of a certain $\hat{\theta}_i$ is zero if $\sum_{k=1}^{N} \frac{\partial y_k^T}{\partial \hat{\theta}_i}\delta y_k = 0$, i.e., if the sensitivity sequence vector of $\hat{\theta}_i$ is orthogonal to the uncertainty sequence vector. This is another important sensitivity structure that dictates the propagation of uncertainty to the estimation error, which is not considered by conventional analysis criteria.
5. The final term $\left(\sum_{k=1}^{N} \frac{\partial y_k^T}{\partial \hat{\boldsymbol{\theta}}}\frac{\partial y_k}{\partial \hat{\boldsymbol{\phi}}}\right)\Delta\boldsymbol{\phi}$ represents the error caused by uncertainty in the non-estimated model parameters ϕ. The associated sensitivity structure $\sum_{k=1}^{N} \frac{\partial y_k^T}{\partial \hat{\boldsymbol{\theta}}}\frac{\partial y_k}{\partial \hat{\boldsymbol{\phi}}}$ is a matrix of inner products between the sensitivity sequence vector of each estimated parameter $\hat{\theta}_i$ and that of each non-estimated parameter $\hat{\phi}_j$, i.e., $\frac{\partial \boldsymbol{y}}{\partial \hat{\theta}_i}$ and $\frac{\partial \boldsymbol{y}}{\partial \hat{\phi}_j}$, which is multiplied by the uncertainty vector $\Delta\boldsymbol{\phi}$. Thus, the influence of $\Delta\boldsymbol{\phi}$ on the total estimation error can be eliminated if $\sum_{k=1}^{N} \frac{\partial y_k^T}{\partial \hat{\boldsymbol{\theta}}}\frac{\partial y_k}{\partial \hat{\boldsymbol{\phi}}} = \mathbf{0}$, where each combination of $\frac{\partial \boldsymbol{y}}{\partial \hat{\theta}_i}$ and $\frac{\partial \boldsymbol{y}}{\partial \hat{\phi}_j}$ is orthogonal. This is an additional sensitivity structure with critical impact on estimation accuracy, which is related to our prior analytical Cramér-Rao bound analysis.[20] The study

indicates that bivariate estimation does not suffer loss of accuracy (increased error covariance) over univariate estimation if the data contain orthogonal sensitivities between parameters.

6. The covariance of the error equation is the Cramér-Rao bound, under the assumptions of unbiased estimation and i.i.d. Gaussian model/measurement noise. Specifically, the assumption of unbiased estimation removes the constant Δy and $\Delta\phi$ terms from Eq. 6, and we represent the varying model/measurement uncertainty as an unbiased Gaussian random variable with covariance Σ, i.e., $\delta\boldsymbol{y} \sim \boldsymbol{N}(\boldsymbol{0}, \Sigma)$. The error is thus linearly related to $\delta\boldsymbol{y}$ as

$$\Delta\boldsymbol{\theta} \sim -\left(\frac{\partial \boldsymbol{y}}{\partial \hat{\boldsymbol{\theta}}}^T \frac{\partial \boldsymbol{y}}{\partial \hat{\boldsymbol{\theta}}}\right)^{-1} \frac{\partial \boldsymbol{y}}{\partial \hat{\boldsymbol{\theta}}}^T \delta\boldsymbol{y}, \quad [8]$$

where $\frac{\partial \boldsymbol{y}}{\partial \hat{\boldsymbol{\theta}}} = \left[\frac{\partial y_1}{\partial \hat{\boldsymbol{\theta}}}; \ldots; \frac{\partial y_N}{\partial \hat{\boldsymbol{\theta}}}\right]$ is the $N \times n$ sensitivity matrix. By linear transformation, the covariance of the estimation error in Eq. 8 is

$$\boldsymbol{cov}(\Delta\boldsymbol{\theta}) = \left(\frac{\partial \boldsymbol{y}}{\partial \hat{\boldsymbol{\theta}}}^T \frac{\partial \boldsymbol{y}}{\partial \hat{\boldsymbol{\theta}}}\right)^{-1} \frac{\partial \boldsymbol{y}}{\partial \hat{\boldsymbol{\theta}}}^T \boldsymbol{\Sigma} \frac{\partial \boldsymbol{y}}{\partial \hat{\boldsymbol{\theta}}} \left(\frac{\partial \boldsymbol{y}}{\partial \hat{\boldsymbol{\theta}}}^T \frac{\partial \boldsymbol{y}}{\partial \hat{\boldsymbol{\theta}}}\right)^{-1}. \quad [9]$$

The assumption of i.i.d. model/measurement noise with variance σ^2, i.e., $\Sigma = \sigma^2\boldsymbol{I}$, yields

$$\boldsymbol{cov}(\Delta\boldsymbol{\theta}) = \left(\frac{1}{\sigma^2} \frac{\partial \boldsymbol{y}}{\partial \hat{\boldsymbol{\theta}}}^T \frac{\partial \boldsymbol{y}}{\partial \hat{\boldsymbol{\theta}}}\right)^{-1}, \quad [10]$$

which is exactly the Cramér-Rao bound,[17,21] i.e., the inverse of the Fisher information matrix. This is significant because it indicates that the Cramér-Rao bound can be achieved for the least-squares objective if the system is unbiased, has i.i.d. Gaussian model/measurement noise, and is linear in its parameters, i.e., the derivatives of the output to each parameter do not exist beyond the first-order. More importantly, this study illustrates the limitations of the Cramér-Rao bound as an analysis criterion, as it exclusively characterizes the estimation (co)variance bound for the limiting case of unbiased estimation. Based on the prior note about the Fisher information matrix, we see that the Fisher information is more generally applicable as an analysis criterion, as it plays a significant role in the error regardless of the presence of bias. Still, the error equation in Eq. 6 provides the most complete expression for the estimation error through consideration of constant and varying system uncertainties.

Li-ion Battery Model & Parameter Sensitivity

This section will briefly summarize the Li-ion battery model, target parameters, and parameter sensitivity associated with our application of analyzing electrochemical parameter estimation errors. Specifically, we will investigate, as a few examples, the estimation of the cathode lithium diffusion coefficient $D_{s,p}$, cathode active material volume fraction $\varepsilon_{s,p}$, anode reaction rate constant k_n, and cathode reaction rate constant k_p, based on the widely-adopted single particle model with electrolyte dynamics (SPMe).[11,35,36] Physically, $D_{s,p}$ characterizes the rate at which lithium ions can diffuse through the cathode electrode particle material, $\varepsilon_{s,p}$ represents the fraction of the total cathode volume capable of storing lithium ions, and k_n and k_p characterize the rates of the (de) intercalation reactions in the anode and cathode, respectively. The involved parameters play a vital role in the performance of the battery and are commonly studied in parameter estimation, especially for SOH monitoring applications,[27,37,38] as they are associated with various degradation mechanisms such as transition metal dissolution,[44,45] reaction-induced mechanical stress,[46,47] and modes of loss of lithium inventory, e.g., solid-electrolyte interphase (SEI) layer growth[38,48] and electrolyte decomposition.[27,49] The model and sample parameters are used in this work as examples for illustrating the methodology of estimation error analysis, which can be applied to other models and parameters without loss of generality.

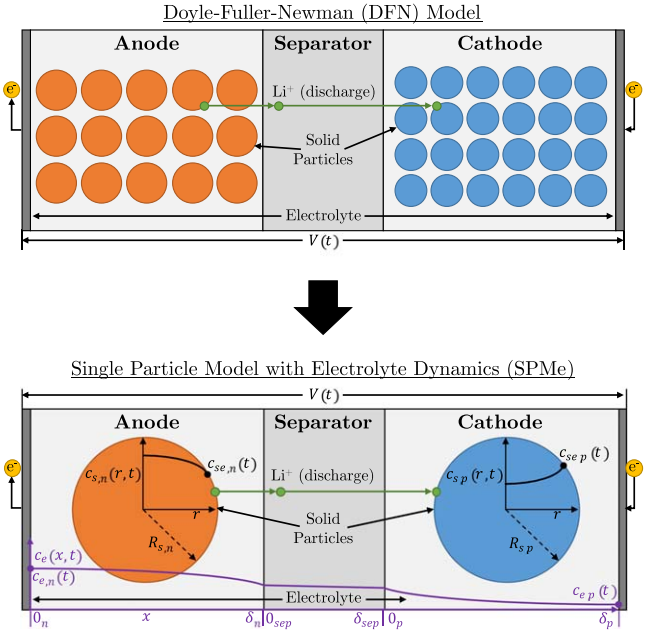

Figure 1. Schematic of DFN model and SPMe.

SPMe reduced-order electrochemical battery model.—The DFN model is the prevailing first-principles battery model, which predicts the output terminal voltage (V) and battery internal physical states from the input current (I) through theoretical representations of electrochemical mechanisms (e.g., lithium diffusion, charge transfer kinetics), according to the porous electrode theory and concentrated solution theory.[34] The model comprises a series of coupled PDEs that impose significant computational expense, motivating the development of explicit reduced-order electrochemical models. One such model is the SPMe, which is well-regarded in the battery control and diagnostics community for its balance between fidelity and computational efficiency.[11,35,36] The SPMe is derived from the DFN model under the fundamental simplification that reaction current density j^{Li} (and thus solid-phase Li-ion concentration) is uniform across each electrode, i.e.,

$$j_i^{Li} = \pm\frac{I}{A_i\delta_i}, \quad [11]$$

where A is the electrode area, δ is the electrode thickness, $\pm$ is $+$ for the anode and $-$ for the cathode (under the convention that current is positive when discharging), and subscript i can be either p or n to denote the cathode or anode, respectively. Accordingly, the electrochemical mechanisms in each electrode (i.e., lithium diffusion and (de)intercalation) are represented with a single particle, and both electrode particles are interfaced with the electrolyte diffusion dynamics across the anode, separator, and cathode, as shown in Fig. 1. Mathematically, the single-particle assumption decouples the governing PDEs of the DFN model, which substantially reduces the computational expense and makes the SPMe suitable for use in real-time applications, e.g., in battery management systems (BMSs).[1] This is facilitated through model-order reduction techniques that enable accurate and computationally-efficient solutions to the decoupled PDEs, e.g., finite difference method[50,51] and Padé approximation.[11,52,53]

The SPMe output terminal voltage is expressed as

$$V = U_p(c_{se,p}) - U_n(c_{se,n}) + \phi_{e,p}(c_{e,p}) - \phi_{e,n}(c_{e,n}) + \eta_p(c_{se,p}, c_{e,p}) - \eta_n(c_{se,n}, c_{e,n}) - IR_l, \quad [12]$$

which includes the difference between the cathode and anode in open-circuit potentials (OCPs) U, electrolyte potentials ϕ_e, and overpotentials η. The OCPs U represent the equilibrium potential

of each electrode as a nonlinear function of the electrode particle surface lithium concentration c_{se}. The evolution of c_{se} is governed by the solid-phase Li-ion diffusion dynamics according to Fick's second law in spherical coordinates,

$$\frac{\partial c_{s,i}}{\partial t}(r,\,t) = D_{s,i}\left(\frac{\partial^2 c_{s,i}}{\partial r^2}(r,\,t) + \frac{2}{r}\frac{\partial c_{s,i}}{\partial r}(r,\,t)\right), \quad [13]$$

where c_s is the lithium concentration at radial distance r from the center of the particle, subject to the symmetry and surface boundary conditions

$$\frac{\partial c_{s,i}}{\partial r}(0,\,t) = 0 \quad \& \quad D_{s,i}\frac{\partial c_{s,i}}{\partial r}(R_{s,i},\,t) = -\frac{j_i^{Li}}{a_{s,i}F}. \quad [14]$$

Here, D_s is the particle lithium diffusion coefficient, R_s is the particle radius, F is the Faraday constant, and $a_s = \frac{3\varepsilon_s}{R_s}$ is the specific interfacial area between the solid and electrolyte phases, where ε_s is the active material volume fraction. Examples of c_s gradients are illustrated in Fig. 1 for the anode and cathode during discharging, with c_{se} denoted at the surface of each particle. To enable the derivation of analytical sensitivity expressions and improve computational efficiency, the evolution of c_{se} can be represented as a transfer function from I to C_{se} via Laplace transform and third-order Padé approximation of Eqs. 13 and 14,

$$C_{se,i}(s) \approx -\frac{7R_{s,i}^4 s^2 + 420D_{s,i}R_{s,i}^2 s + 3465D_{s,i}^2}{s(R_{s,i}^4 s^2 + 189D_{s,i}R_{s,i}^2 s + 3465D_{s,i}^2)} \cdot \frac{I(s)}{F\varepsilon_{s,i}A_i\delta_i}, \quad [15]$$

which can be conveniently implemented in the time domain through conversion to a linear state-space representation.

The electrolyte potentials ϕ_e are driven by the ionic concentration gradient across the electrolyte, which is characterized by the electrolyte lithium concentration at each electrode boundary c_e. The evolution of c_e is governed by the Li-ion diffusion dynamics in the electrolyte according to Fick's second law in 1D Cartesian coordinates, and an example c_e gradient is illustrated in Fig. 1. Similar to Eq. 15, a rational transfer function from I to C_e can be derived from the diffusion equation via Laplace transform and Padé approximation.

The overpotentials η drive the (de)intercalation reaction current densities according to the Butler-Volmer equation, which, through the single-particle assumption in Eq. 11, can be rearranged as

$$\eta_i = \frac{RT}{\alpha F}\ln\left[\frac{j_i^{Li}}{2a_{s,i}i_{0,i}} + \sqrt{\left(\frac{j_i^{Li}}{2a_{s,i}i_{0,i}}\right)^2 + 1}\right], \quad [16]$$

with

$$i_{0,i} = Fk_i c_e^{\alpha_n}(c_{s,i}^{max} - c_{se,i})^{\alpha_n} c_{se,i}^{\alpha_p}. \quad [17]$$

Above, R is the universal gas constant, T is the temperature, i_0 is the exchange current, k is the reaction rate constant, c_s^{max} is the maximum solid-phase concentration, and α is the charge transfer coefficient, which is assumed to be the same for the cathode and anode ($\alpha = \alpha_p = \alpha_n$).

Finally, the voltage drop across the various Ohmic resistances (i.e., of the SEI layer, electrolyte, and current collectors) is incorporated through the lumped resistance term R_l. The reader is referred to Ref. 11 for the full details of the model.

Parameter sensitivity.—The estimation error equation in Eq. 6 relies upon the sensitivities of the estimated and non-estimated parameters. We employ the analytical sensitivity expressions derived for the SPMe in Ref. 11, which efficiently capture the dynamics of the sensitivity through sensitivity transfer functions (STFs). In general, STFs characterize the mapping of the measured input data to the dynamic sensitivity terms. They are derived based on the model that is used for estimation, i.e., the SPMe in this case, and can be conveniently used to compute the sensitivity, which cannot be measured directly. For example, the sensitivity of the output voltage V to $\varepsilon_{s,p}$ can be derived by taking the partial derivative of Eq. 12 with respect to $\varepsilon_{s,p}$, i.e.,

$$\frac{\partial V}{\partial \varepsilon_{s,p}}(t) = -\frac{\partial R_l}{\partial \varepsilon_{s,p}}I + \frac{\partial \eta_p}{\partial a_{s,p}}\frac{\partial a_{s,p}}{\partial \varepsilon_{s,p}} + \left(\frac{\partial \eta_p}{\partial c_{se,p}} + \frac{\partial U_p}{\partial c_{se,p}}\right)\cdot\frac{\partial c_{se,p}}{\partial \varepsilon_{s,p}}(t). \quad [18]$$

The first term reflects the non-dynamic sensitivity of R_l to $\varepsilon_{s,p}$, which is constant. The second term represents the non-dynamic sensitivity of η_p to $\varepsilon_{s,p}$ through $a_{s,p}$, which can be easily obtained from the model as a nonlinear function of current. The third term expresses the dynamic sensitivity of η_p and U_p to $\varepsilon_{s,p}$ through solid-phase diffusion in the cathode. Specifically, $\frac{\partial \eta_p}{\partial c_{se,p}}$ and $\frac{\partial U_p}{\partial c_{se,p}}$ are the slopes of the overpotential and OCP, while $\frac{\partial c_{se,p}}{\partial \varepsilon_{s,p}}(t)$ is the dynamic sensitivity of $c_{se,p}$ to $\varepsilon_{s,p}$. The dynamics of $\frac{\partial c_{se,p}}{\partial \varepsilon_{s,p}}(t)$ can be captured with an STF by taking the partial derivative of the C_{se} transfer function in Eq. 15 with respect to $\varepsilon_{s,p}$, i.e.,

$$\frac{\partial C_{se,p}}{\partial \varepsilon_{s,p}}(s) = \frac{7R_{s,p}^4 s^2 + 420D_{s,p}R_{s,p}^2 s + 3465D_{s,p}^2}{s(R_{s,p}^4 s^2 + 189D_{s,p}R_{s,p}^2 s + 3465D_{s,p}^2)} \cdot \frac{I(s)}{F\varepsilon_{s,p}^2 A_p\delta_p}. \quad [19]$$

As with Eq. 15, the STF in Eq. 19 can be readily implemented in the time domain by converting to a linear state-space representation.

The $D_{s,p}$ sensitivity expression can be derived in the same way as

$$\frac{\partial V}{\partial D_{s,p}}(t) = \left(\frac{\partial \eta_p}{\partial c_{se,p}} + \frac{\partial U_p}{\partial c_{se,p}}\right)\cdot\frac{\partial c_{se,p}}{\partial D_{s,p}}(t), \quad [20]$$

which relies entirely upon the diffusion dynamics through $c_{se,p}$. The STF for the dynamic sensitivity $\frac{\partial c_{se,p}}{\partial D_{s,p}}(t)$ can be obtained by taking the partial derivative of the C_{se} transfer function in Eq. 15 with respect to $D_{s,p}$, i.e.,

$$\frac{\partial C_{se,p}}{\partial D_{s,p}}(s) = \frac{43R_{s,p}^4 s^2 + 1980D_{s,p}R_{s,p}^2 s + 38115D_{s,p}^2}{(R_{s,p}^4 s^2 + 189D_{s,p}R_{s,p}^2 s + 3465D_{s,p}^2)^2} \cdot \frac{21R_{s,p}^2 I(s)}{F\varepsilon_{s,p}A_p\delta_p}. \quad [21]$$

Finally, the same procedure can be applied to derive an expression for the k sensitivity,

$$\frac{\partial V}{\partial k_i} = \pm\frac{RT}{\alpha F k_i}\cdot\frac{\text{sign}(j_i^{Li})}{\sqrt{1 + \left(\frac{2a_{s,i}i_{0,i}}{j_i^{Li}}\right)^2}}, \quad [22]$$

where $\pm$ is $+$ for the anode and $-$ for the cathode. The k sensitivity in Eq. 22 differs from that of $\varepsilon_{s,p}$ and $D_{s,p}$ because it is entirely non-dynamic, i.e., it is computed from the instantaneous input without dependence on the input history. Thus, Eq. 22 can be directly

implemented without needing to derive an STF. The reader is referred to Ref. 11 for the derivation details and sensitivity expressions for the other parameters.

Univariate Estimation Error Analysis

We will first present the estimation error analysis for the univariate case. Equation 6 will be applied to two univariate battery electrochemical parameter estimation problems with the purpose of validating the error equation and analyzing the composition of error sources due to different types of uncertainty. In this context, the output y is voltage V and the input u is current I. Each estimation is performed with the least-squares algorithm, SPMe battery model, and input-output data sets acquired through experimental testing of an LGM50T INR21700 Li-Nickel-Manganese-Cobalt (NMC) cell, using an Arbin LBT21084 cycler. Three dissimilar input current profiles were applied to the cell, namely, a constant 1C discharge (1C CC), 1C Pulse (1/60 Hz square wave), and the Federal Urban Driving Schedule drive-cycle (FUDS). Each profile has the same duration (30 min) and number of data points (6,000), and the initial cell state of charge (SOC) was 75% for the 1C CC profile and 50% for the 1C Pulse and FUDS profiles. The true parameter set was adopted from Ref. 54, which experimentally parameterized an LGM50 INR21700 cell through a full tear-down analysis. To incorporate the subtle differences between this parameterized LGM50 cell and our LGM50T cell, several parameter values were adjusted according to Ref. 8.

Both estimation scenarios are subject to parameter uncertainty $\Delta\boldsymbol{\phi}$, which characterizes the deviation between the true and assumed values of the non-estimated parameters. In addition, both scenarios are inherently subject to varying model/measurement uncertainty δV_k, which characterizes the mismatch between the measured and modeled (under the true parameter values) outputs. Note that δV_k is the total varying model/measurement uncertainty, i.e., the sum of the constant (Δy) and varying (δy_k) components introduced in the derivation. Figures 2 and 3 provide example visualizations of the model/measurement uncertainty for the 1C CC and FUDS input profiles, where Figs. 2a and 3a compare the measured and modeled voltage outputs, and Figs. 2b and 3b show the corresponding δV_k trajectories. Physically, the varying model/measurement uncertainty corresponds to discrepancies between the modeled and measured output dynamics, which are strongly dependent on the operating conditions, e.g., input current and battery states. Figures 2b and 3b illustrate this dependence, as δV_k under 1C CC (Fig. 2b) is more biased with larger amplitudes and lower-frequency fluctuations, whereas δV_k under FUDS (Fig. 3b) is only slightly biased with relatively small amplitudes and high-frequency fluctuations. The time-varying nature of δV_k makes the estimation problem both challenging and interesting.

The first scenario estimates the cathode active material volume fraction $\varepsilon_{s,p}$ subject to intrinsic model/measurement uncertainty and parameter uncertainty in the separator electrolyte porosity $\varepsilon_{e,sep}$ and cathode lithium diffusion coefficient $D_{s,p}$, i.e., $\theta = \varepsilon_{s,p}$ and $\boldsymbol{\phi} = [\varepsilon_{e,sep}, D_{s,p}]^T$. Parameter uncertainty was applied by scaling $\varepsilon_{e,sep}$ and $D_{s,p}$ by 20% from the true values. For this scenario, the general form of the error equation in Eq. 6 is cast as

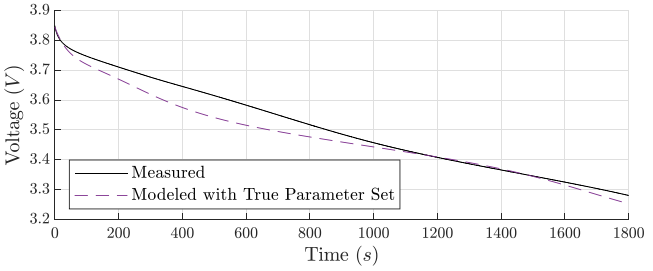

(a) Comparison of measured and modeled (under true parameter set) voltage outputs.

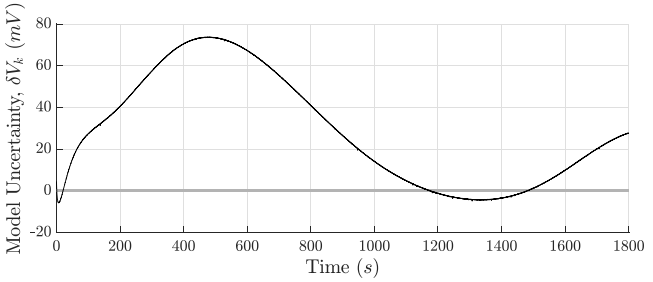

(b) Model/measurement uncertainty δV_k computed as difference between measured and modeled voltage outputs from (a).

Figure 2. Model/measurement uncertainty under 1C CC input profile.

Fig. 4 under each input profile. These plots indicate that parameter sensitivity is strongly dependent on the input data, as the sensitivities under the 1C CC profile have significantly larger amplitudes than those under the other profiles. In addition, the sensitivity trajectories for these parameters tend to be similar in structure to the associated input excitations, i.e., the sensitivities under 1C CC are nearly constant (or have a constant slope), those under 1C Pulse oscillate at a constant frequency, and those under FUDS feature sporadic high-frequency fluctuations. Finally, we see that the $\varepsilon_{s,p}$ and $D_{s,p}$ sensitivities under 1C Pulse are approximately mirrored across the horizontal axis (albeit with a considerable amplitude disparity), which are examples of semi-orthogonal sensitivity structures that will reduce the influence of parameter uncertainty on the estimation error, e.g., according to the third numerator term in Eq. 23. Note also that orthogonality between the $\varepsilon_{s,p}$ sensitivity and δV_k trajectory (example δV_k trajectories are shown in Figs. 2b and 3b) will mitigate the influence of model/measurement uncertainty on the estimation error, according to the first numerator term in Eq. 23.

The estimation was performed for each input current profile and the results are summarized in Table I. Specifically, the actual error is the true error between the estimate and the benchmark value, while the predicted error was computed from the error equation in Eq. 23. The normalized Fisher information $\overline{F}_{info}$ is also included, which is the denominator of Eq. 23 times $\hat{\varepsilon}_{s,p}^2$. The next three columns indicate the

$$\Delta\varepsilon_{s,p} = -\frac{\left(\sum_{k=1}^{N}\frac{\partial V_k}{\partial\hat{\varepsilon}_{s,p}}\delta V_k\right) + \left(\sum_{k=1}^{N}\frac{\partial V_k}{\partial\hat{\varepsilon}_{s,p}}\frac{\partial V_k}{\partial\hat{\varepsilon}_{e,sep}}\right)\Delta\varepsilon_{e,sep} + \left(\sum_{k=1}^{N}\frac{\partial V_k}{\partial\hat{\varepsilon}_{s,p}}\frac{\partial V_k}{\partial\hat{D}_{s,p}}\right)\Delta D_{s,p}}{\sum_{k=1}^{N}\left(\frac{\partial V_k}{\partial\hat{\varepsilon}_{s,p}}\right)^2}, \quad [23]$$

where the denominator is the Fisher information of $\varepsilon_{s,p}$ and the numerator contains the uncertainty terms, δV_k, $\Delta\varepsilon_{e,sep}$, and $\Delta D_{s,p}$. To visualize the parameter sensitivity terms, the normalized sensitivities under the true parameter set, i.e., $\frac{\partial V_k}{\partial\boldsymbol{\phi}} = \boldsymbol{\phi}\frac{\partial V_k}{\partial\boldsymbol{\phi}}$, are shown in

error contributions of each uncertainty, according to Eq. 23. For example, the error contribution of $D_{s,p}$ is the third term in the numerator divided by the denominator. Finally, the last three columns list the root-mean-square (RMS) values of the model/

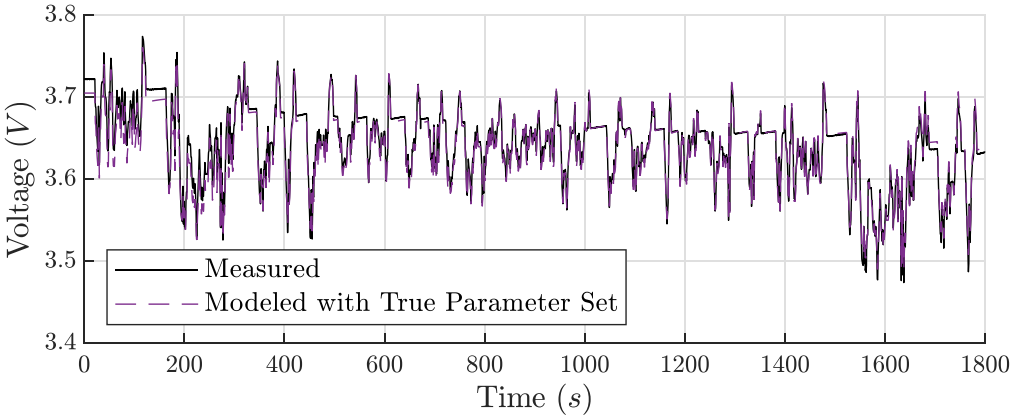

(a) Comparison of measured and modeled (under true parameter set) voltage outputs.

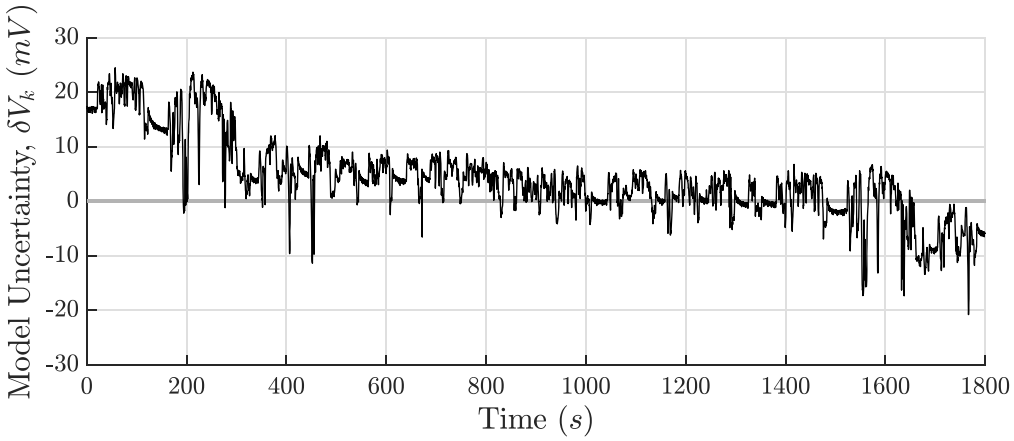

(b) Model/measurement uncertainty δV_k computed as difference between measured and modeled voltage outputs from (a).

Figure 3. Model/measurement uncertainty under FUDS input profile.

measurement uncertainty δV_k and normalized sensitivities of the uncertain parameters, i.e., $\frac{\partial \overline{V_k}}{\partial \hat{\phi}} = \hat{\phi}\frac{\partial V_k}{\partial \hat{\phi}}$. In addition to Table I, we provide a visual comparison of the error contributions of each uncertainty in Fig. 5.

The second scenario estimates $D_{s,p}$ subject to intrinsic model/measurement uncertainty and parameter uncertainty in the anode lithium diffusion coefficient $D_{s,n}$ and $\varepsilon_{s,p}$. In this case, the assumed values of $D_{s,n}$ and $\varepsilon_{s,p}$ were selected to be 10% larger than the true values. The error equation for this scenario follows the same form as Eq. 23, with $\varepsilon_{s,p}$, $\varepsilon_{e,sep}$, and $D_{s,p}$ replaced with $D_{s,p}$, $D_{s,n}$, and $\varepsilon_{s,p}$, respectively. The results are summarized in Table II under the same organization as Table I, and the error contributions of each uncertainty are compared in Fig. 6.

Tables I and II indicate that the predicted errors agree well with the actual errors, validating the error equation in Eq. 6. An important observation is that the deviations between the predicted and actual errors increase at larger actual errors. This is due to the first-order Taylor series in Eq. 5, which was used to expand the model output under the true parameter set ($\boldsymbol{\theta}$, ϕ) about the estimated/assumed parameter set ($\hat{\boldsymbol{\theta}}$, $\hat{\boldsymbol{\phi}}$). Since the accuracy of the expansion (and thus the error equation) is dependent on the proximity of the estimated/assumed parameter set to the true parameter set, prediction accuracy increases as the estimate of the target parameter approaches the true value, i.e., when the actual error is small. From a practical standpoint, we are typically not concerned with error prediction accuracy if the estimate is poor, yet even when this is the case, the error equation can still discern between high- and low-accuracy results, i.e., predicted errors are still large when actual errors are large, and small when actual errors are small.

A second observation is that the Fisher information is not necessarily correlated with the estimation error. For example, the 1C Pulse and FUDS results in Table I have the smallest and largest errors with nearly equivalent Fisher information values. In addition, the 1C CC Fisher information values in Tables I and II are two orders of magnitude larger than those of FUDS, yet the estimation errors for 1C CC are larger. This highlights the limitations of the Fisher information as a standalone metric for data quality, though it is still intrinsic to the estimation error, as Eq. 23 indicates that it is related to the robustness of the error against the uncertainty-propagating numerator terms. Even so, the system uncertainties play a significant role in the total error and should not be ignored.

Third, Tables I and II show that the estimation error is strongly dependent on the data. This is because the model/measurement uncertainty and parameter sensitivities are dynamically driven by the input, e.g., as characterized by the STFs discussed earlier and

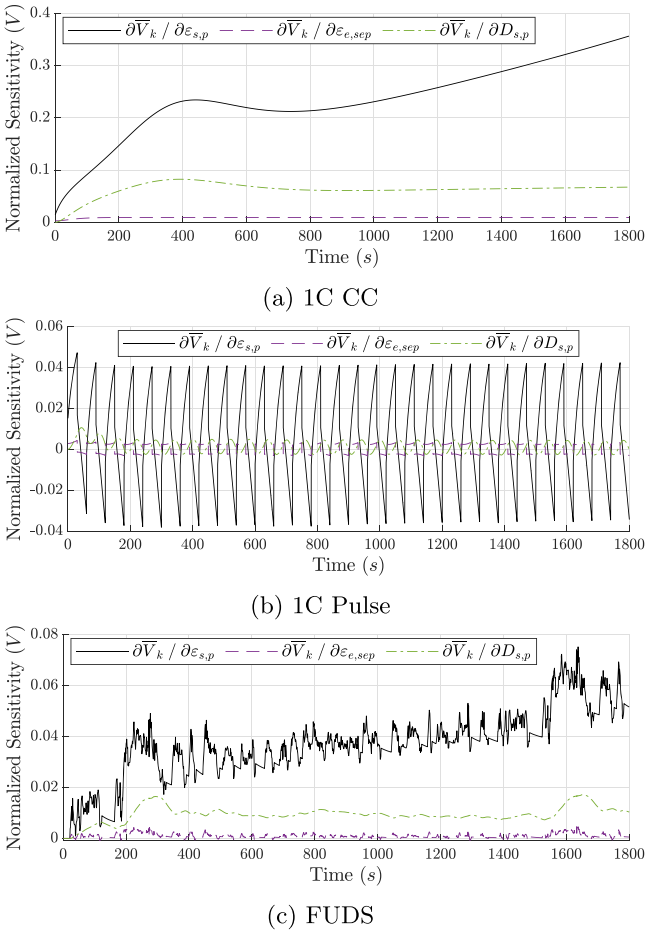

Figure 4. Comparison of normalized $\varepsilon_{s,p}$, $\varepsilon_{e,sep}$, and $D_{s,p}$ sensitivities under true parameter set and different input profiles.

visualized in Figs. 2–4. It follows that the error contribution of each uncertainty is also dependent on the data, as observed by the large variations across Figs. 5 and 6. For example, the dominant uncertainty in Fig. 6 is the model/measurement uncertainty δV_k under 1C CC and 1C Pulse, but the parameter uncertainty $\Delta\varepsilon_{s,p}$ is (slightly) dominant under FUDS. In most cases, the uncertain parameter with the highest sensitivity has the largest error contribution, e.g., in Table II, $\varepsilon_{s,p}$ has a higher RMS sensitivity and error contribution than $D_{s,n}$ for every input profile. This aligns with the conventional sensitivity analysis criterion, which specifies that the most sensitive parameter will have the greatest influence on the estimation result. However, the influence of a parameter may not always be reflected by its sensitivity, as Table I reveals that $D_{s,p}$ is always more sensitive than $\varepsilon_{e,sep}$ (by at least a factor of two), though $\varepsilon_{e,sep}$ has a larger error contribution under 1C Pulse. This is due to the uncertainty-propagating sensitivity structures, e.g., $\sum_{k=1}^{N} \frac{\partial y_k}{\partial \hat{\theta}} \frac{\partial y_k}{\partial \hat{\phi}}$, which can amplify or attenuate the influence of an uncertain parameter based on the orthogonality of its sensitivity to that of

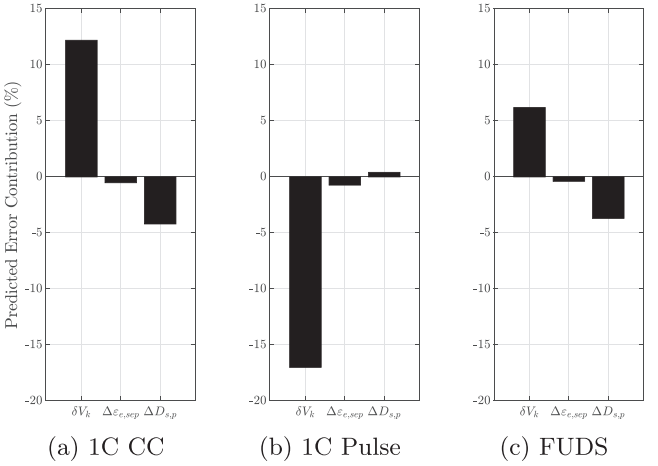

Figure 5. Predicted error contributions of model/measurement uncertainty δV_k, parameter uncertainty in $\varepsilon_{e,sep}$, and parameter uncertainty in $D_{s,p}$ for estimation of $\varepsilon_{s,p}$ under different input profiles.

the target parameter. Another example of uncertainty propagation is in Table II, where the δV_k error contribution under 1C Pulse is significantly higher than that of 1C CC, yet the δV_k RMS value is lower. Thus, the 1C Pulse profile has amplified the influence of δV_k through the associated uncertainty-propagating sensitivity structure. Therefore, parameter sensitivity magnitude is not sufficient as a standalone criterion for data quality—the uncertainty-propagating sensitivity structures are also critical.

Finally, we see that it is possible for (partial) cancellation to occur between different error contributions. This is most notable for $D_{s,p}$ estimation under the FUDS profile (Fig. 6c), where the δV_k contribution of 29.9% almost completely cancels with the combined parameter uncertainty contribution of -32%, yielding a total predicted error of -2.1% (which nearly matches the actual error of -4.8% in Table II). Had there been no model/measurement uncertainty or parameter uncertainty for this case, the estimation error would have been much larger. This cancellation phenomenon is entirely fortuitous, and may explain why sometimes unexpectedly small estimation errors are observed under large system uncertainties. It can also be misleading in error analysis, as low-quality data can be wrongly associated with high estimation accuracy if there is significant error cancellation. In this case, the estimation error can drastically increase if the signs of the uncertainties change, which are unknown and uncontrollable in practice. Therefore, it is recommended to examine the worst-case scenario of purely additive uncertainty (e.g., by taking the absolute value of each numerator term in Eq. 7) when using the error equation to evaluate data quality, as was done in Refs. 32, 33.

Bivariate Estimation Error Analysis

We will now present the estimation error analysis for the bivariate case. The error equation in Eq. 6 will be applied to two bivariate estimation scenarios to validate the multivariate form of the error equation, analyze the effects of simultaneously estimating multiple parameters under the same data, and examine the identifiability of the parameters.

Table I. Univariate estimation of $\varepsilon_{s,p}$ subject to uncertainty in $\varepsilon_{e,sep}$ and $D_{s,p}$.

				Predicted Error Contribution			RMS Values (mV)		
Input Profile	Actual Error	Predicted Error	$\overline{F}_{info}$ (V^2)	δV_k	$\Delta\varepsilon_{e,sep}$	$\Delta D_{s,p}$	δV_k	$\frac{\partial \overline{V}_k}{\partial \hat{\varepsilon}_{e,sep}}$	$\frac{\partial \overline{V}_k}{\partial \hat{D}_{s,p}}$
1C CC	6.2%	7.5%	273	12.2%	−0.52%	−4.2%	38.8	6.8	55.3
1C Pulse	−22.3%	−17.3%	8.3	−17.0%	−0.73%	0.41%	21.5	2.0	4.3
FUDS	1.3%	2.1%	8.1	6.2%	−0.39%	−3.7%	8.4	1.0	8.6

Table II. Univariate estimation of $D_{s,p}$ subject to uncertainty in $D_{s,n}$ and $\varepsilon_{s,p}$.

				Predicted Error Contribution			RMS Values (mV)		
Input Profile	Actual Error	Predicted Error	$\overline{F}_{info}$ (V^2)	δV_k	$\Delta D_{s,n}$	$\Delta\varepsilon_{s,p}$	δV_k	$\frac{\partial \overline{V}_k}{\partial \hat{D}_{s,n}}$	$\frac{\partial \overline{V}_k}{\partial \hat{\varepsilon}_{s,p}}$
1C CC	18.3%	25.7%	12.8	68.6%	−0.68%	−42.3%	38.8	5.2	221
1C Pulse	349%	463%	0.0082	529%	−0.47%	−65.9%	21.5	0.087	20.6
FUDS	−4.8%	−2.1%	0.60	29.9%	−0.081%	−31.9%	8.4	0.12	36.5

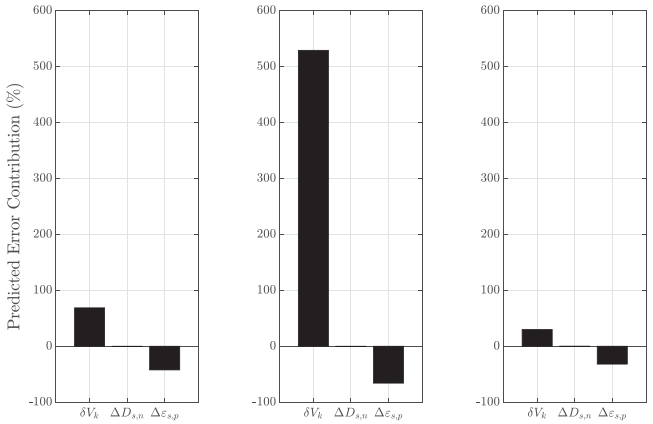

Figure 6. Predicted error contributions of model/measurement uncertainty δV_k, parameter uncertainty in $D_{s,n}$, and parameter uncertainty in $\varepsilon_{s,p}$ for estimation of $D_{s,p}$ under different input profiles.

Influence of estimating multiple parameters.—In this first bivariate estimation scenario, we study the effects of adding a second target parameter to the estimation under the same data. The estimation procedure is identical to that of the univariate estimation, except that two parameters are estimated instead of one, namely, $\varepsilon_{s,p}$ and the anode reaction rate constant k_n, giving $\boldsymbol{\theta} = [\varepsilon_{s,p}, k_n]^T$. Accordingly, the error equation in Eq. 6 is cast as

$$\Delta\varepsilon_{s,p} = \frac{\left(\sum_{k=1}^{N}\frac{\partial V_k}{\partial\hat{\varepsilon}_{s,p}}\frac{\partial V_k}{\partial\hat{k}_n}\right)\left(\sum_{k=1}^{N}\frac{\partial V_k}{\partial\hat{k}_n}\delta V_k\right) - \sum_{k=1}^{N}\left(\frac{\partial V_k}{\partial\hat{k}_n}\right)^2\left(\sum_{k=1}^{N}\frac{\partial V_k}{\partial\hat{\varepsilon}_{s,p}}\delta V_k\right)}{\sum_{k=1}^{N}\left(\frac{\partial V_k}{\partial\hat{\varepsilon}_{s,p}}\right)^2\sum_{k=1}^{N}\left(\frac{\partial V_k}{\partial\hat{k}_n}\right)^2 - \left(\sum_{k=1}^{N}\frac{\partial V_k}{\partial\hat{\varepsilon}_{s,p}}\frac{\partial V_k}{\partial\hat{k}_n}\right)^2} \quad [24]$$

for the error in $\varepsilon_{s,p}$, while the k_n error equation follows a symmetric form. The only uncertainty considered here is the model/measurement uncertainty δV_k, as both parameters $\varepsilon_{s,p}$ and k_n are being estimated simultaneously. When compared with the univariate form, the bivariate error equation in Eq. 24 features a more complicated uncertainty-propagating sensitivity structure in the numerator and the determinant of the Fisher information matrix in the denominator.

The bivariate estimation results are summarized in Table III, where the predicted errors are presented alongside the actual errors for both parameters. The normalized determinant of the Fisher information matrix $|\overline{\boldsymbol{F}}_{info}|$ is also listed. For comparison, the univariate estimation results are included, where $\varepsilon_{s,p}$ and k_n were each independently estimated subject to model/measurement uncertainty and uncertainty in the respective non-estimated parameter, realized by a 20% deviation from the true value. The actual error, predicted error, and normalized Fisher information are listed for each case.

Table III first indicates that the actual and predicted errors mostly show good agreement for the bi- and univariate estimations, which further validates the error equation. However, exceptions occur in the bivariate results for $\varepsilon_{s,p}$ under 1C Pulse and k_n under 1C CC, which have significantly larger predicted errors than actual errors, i.e., 700% vs 224% and 4004% vs 724%, respectively. This is because the first-order Taylor expansion in Eq. 5 causes error prediction accuracy to degrade when the actual error is large, as discussed in the univariate estimation analysis. Nevertheless, even at large actual errors, the error equation is still effective at discerning the quality of data, i.e., large predicted errors are associated with large actual errors.

Second, the bivariate Fisher information is not necessarily correlated with the estimation error. For example, the bivariate Fisher information values under 1C CC and 1C Pulse are nearly equivalent, yet the $\varepsilon_{s,p}$ error is significantly larger under 1C Pulse, while the k_n error is larger under 1C CC. In addition, both univariate estimation cases under FUDS in Table III have the smallest errors despite having the smallest Fisher information values. These observations align with those of the earlier univariate estimation analysis and reinforce that the Fisher information is limited as a standalone criterion for data quality, as the system uncertainties play a significant role in the total error and should be considered in error analysis.

Finally, the results in Table III reveal that simultaneously estimating two parameters can yield larger errors than estimating each parameter independently (albeit subject to the uncertainty in the non-estimated parameter), under the same data. Specifically, we see that each bivariate estimation error is larger than the corresponding univariate estimation error, even though the former is not subject to parameter uncertainty through the inclusion of the unknown parameter in the estimation. This can be explained by examining the form of the $\varepsilon_{s,p}$ bivariate error equation in Eq. 24. Specifically, dividing the numerator and denominator of Eq. 24 by $\sum_{k=1}^{N}\left(\frac{\partial V_k}{\partial\hat{k}_n}\right)^2$ yields the new denominator, $\sum_{k=1}^{N}\left(\frac{\partial V_k}{\partial\hat{\varepsilon}_{s,p}}\right)^2 - \frac{\left(\sum_{k=1}^{N}\frac{\partial V_k}{\partial\hat{\varepsilon}_{s,p}}\frac{\partial V_k}{\partial\hat{k}_n}\right)^2}{\sum_{k=1}^{N}\left(\frac{\partial V_k}{\partial\hat{k}_n}\right)^2}$, which is the denominator of the univariate estimation error equation in Eq. 23 minus a positive term. Thus, the denominator always diminishes under the bivariate estimation case. Therefore, simultaneously estimating a second parameter causes the bivariate estimation to be less robust than the univariate case to the influence of system uncertainties, characterized by the numerator. This aligns with the results in Refs. 19–21, in which the Cramér-Rao bound was analytically derived for numerous unbiased estimation scenarios, showing that the error (co)variance for multivariate estimation can never be less than that of univariate estimation, under the same data.

Parameter identifiability.—Since the multivariate estimation of electrochemical battery parameters is often susceptible to identifiability issues,[7,41] we present a second bivariate estimation scenario to examine the identifiability of two parameters under different data. The estimation procedure is the same as that of the previous scenario, except that $\varepsilon_{s,p}$ is estimated alongside the cathode reaction rate constant k_p, instead of k_n. The actual errors, predicted errors, and normalized determinants of the Fisher information matrix are summarized in Table IV.

The results in Table IV reinforce the insights from the preceding sections. Specifically, error prediction accuracy is highest when the

Table III. Bivariate vs univariate estimation of $\varepsilon_{s,p}$ and k_n.

	Bivariate Estimation of $\varepsilon_{s,p}$ and k_n					Univariate Estimation of $\varepsilon_{s,p}$ subject to Uncertainty in k_n			Univariate Estimation of k_n subject to Uncertainty in $\varepsilon_{s,p}$		
Input Profile	$\varepsilon_{s,p}$ Act. Error	$\varepsilon_{s,p}$ Pred. Error	k_n Act. Error	k_n Pred. Error	$\lvert\overline{F}_{info}\rvert$ (V^4)	Act. Error	Pred. Error	$\overline{F}_{info}$ (V^2)	Act. Error	Pred. Error	$\overline{F}_{info}$ (V^2)
1C CC	−13.8%	−11.9%	724%	4004%	0.85	7.9%	8.8%	274	−21.5%	−9.5%	22.9
1C Pulse	224%	700%	−44.3%	−31.5%	0.66	−35.7%	−22.3%	16.6	−32.8%	−25.5%	32.3
FUDS	1.0%	1.0%	16.9%	19.0%	11.5	0.23%	1.0%	9.0	−0.011%	2.5%	3.1

Table IV. Bivariate estimation of $\varepsilon_{s,p}$ and k_p.

Input Profile	$\varepsilon_{s,p}$ Actual Error	$\varepsilon_{s,p}$ Predicted Error	k_p Actual Error	k_p Predicted Error	$\lvert\overline{F}_{info}\rvert$ (V^4)
1C CC	5.1%	−6.2%	9.1×10^{14}%	2.3×10^{28}%	2.5×10^{-51}
1C Pulse	225%	703%	−86.8%	−36.8%	4.0
FUDS	2.7%	2.7%	114%	250%	0.032

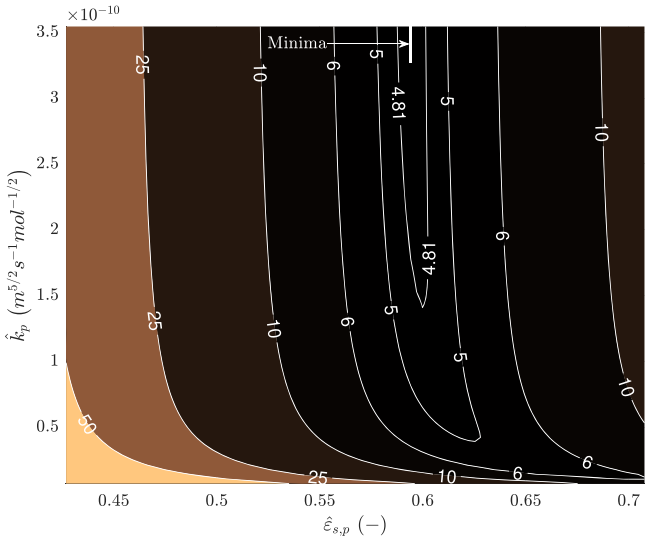

(a) Sum of squared errors (V^2) under 1C CC input profile.

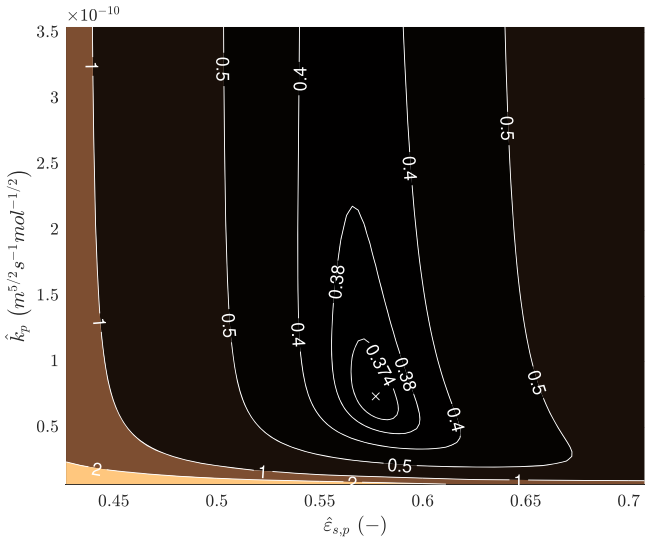

(b) Sum of squared errors (V^2) under FUDS input profile.

Figure 7. Sum of squared errors for bivariate estimation of $\varepsilon_{s,p}$ and k_p.

actual error is small (due to the Taylor series expansion in the derivation of the error equation) and estimation accuracy is strongly dependent on the data. Additionally, the Fisher information is not necessarily correlated with the estimation error, e.g., the error in $\varepsilon_{s,p}$ is significantly smaller under FUDS than under 1C Pulse, yet the Fisher information value under FUDS is two orders of magnitude smaller.

Regarding the identifiability of the parameters, Table IV indicates that the least-squares algorithm returned reasonable (albeit generally large) errors for both parameters under 1C Pulse and FUDS. However, identifiability issues emerged under 1C CC, in which the $\varepsilon_{s,p}$ error is relatively small (5.1%) while the k_p error is extremely large (9.1×10^{14}%). This further reinforces that estimation accuracy is strongly dependent on data, which we illustrate in Fig. 7 through contour plots of the estimation cost surface (i.e., sum of squared errors) across different target parameter values under the 1C CC (Fig. 7a) and FUDS (Fig. 7b) input profiles. Figure 7b shows that a global minimum exists under the FUDS profile (denoted by the ×), which corresponds to unique identifiability of both parameters. However, Fig. 7a reveals that estimation under 1C CC yields a line of minima along the valley bounded by the 4.81 V^2 contour. Since this valley extends along the $\hat{k}_p$-axis, k_p is not uniquely identifiable despite unique identifiability in $\varepsilon_{s,p}$, which is reflected in Table IV by the large error in k_p and relatively small error in $\varepsilon_{s,p}$. Table IV also indicates that the Fisher information determinant is essentially zero under 1C CC, which aligns with the conventional criterion that some portion of the target parameters are not uniquely identifiable if the Fisher information matrix is singular.[17,43] Since the Fisher information matrix is inverted in the error equation, the error equation becomes ill-posed under the 1C CC profile. Regardless, the predicted error is still small for $\varepsilon_{s,p}$ and very large for k_p, which is consistent with the identifiability of $\varepsilon_{s,p}$ and lack of identifiability of k_p observed in Fig. 7a. Thus, even if the estimation problem is ill-posed with nonunique parameter identifiability, the error equation may still be capable of discerning which parameter is not uniquely identifiable.

Conclusions

In this paper, a generalized multivariate estimation error equation was derived under the least-squares objective function not subject to the limitations of conventional analysis criteria, i.e., unbiased estimation and omission of system uncertainties. Analysis of the equation revealed the sensitivity structures that propagate various types of system uncertainties to the estimation error, and that estimation accuracy depends more on data quality than quantity. The error equation was validated through comparison of the predicted and actual errors in a series of uni- and bivariate battery electrochemical parameter estimation scenarios. These analyses highlighted the strong dependence of the estimation error (and its decomposition into the impact of different uncertainties) on data and the limitations of the conventional error analysis criteria. Specifically, parameter sensitivity magnitude alone does not determine the influence of uncertainties on the estimation result, as the uncertainty-propagating sensitivity structures are critical; the Fisher information is an important term in the error equation associated with robustness to general system uncertainties, yet it is only part of the equation and cannot serve as a standalone metric for data quality—the system uncertainties must be considered; and the Cramér-Rao bound is not as widely applicable as the Fisher information as an error analysis criterion due to the restrictive assumption of unbiased estimation, as bias is inevitable in practice. Finally, the bivariate error analysis demonstrated that the error equation can discern the identifiability of the target parameters and revealed that simultaneously estimating a second parameter under the same data intrinsically reduces the error robustness to system uncertainties.

The insights provided by the proposed error analysis method can facilitate more-informed and better-designed parameter estimation practices, which are critical for interpreting and predicting the physical phenomena associated with battery performance. In particular, the accurate estimation of health-related parameters provides a

noninvasive and real-time indication of battery degradation and remaining useful life, which are very important in practice. On this front, we have been trying to leverage the insights from error analysis to select the best data segments from an existing database or online data stream for estimating the battery health-related parameters.[32,33] Additionally, a properly parameterized model can be used for prognostics and predictive control by leveraging the capability of the model (with estimated parameters) to predict future battery performance—a necessary feature for advanced battery management. On this front, we have been exploring the use of the favorable data structures identified from the error equation to formulate objectives for input excitation design, to improve the model parameterization accuracy.[8] Lastly, it is noted that the proposed error analysis method can be applied to a broad range of works on battery parameter estimation in literature, as most existing works use the least-squares objective (not just limited to the original ordinary least-squares algorithm).

Acknowledgments

We appreciate the funding support from the NSF CAREER Program (Grant No. 2046292) and the NASA HOME Space Technology Research Institute (Grant No. 80NSSC19K1052).

ORCID

Jackson Fogelquist https://orcid.org/0000-0001-8199-3507
Qingzhi Lai https://orcid.org/0000-0002-7077-2132
Xinfan Lin https://orcid.org/0000-0002-2929-8563

References

1. X. Lin, Y. Kim, S. Mohan, J. B. Siegel, and A. G. Stefanopoulou, "Modeling and estimation for advanced battery management." *Annual Review of Control, Robotics, and Autonomous Systems*, **2**, 393 (2019).
2. Z. Khalik, M. C. F. Donkers, J. Sturm, and H. J. Bergveld, "Parameter estimation of the Doyle-Fuller-Newman model for lithium-ion batteries by parameter normalization, grouping, and sensitivity analysis." *J. Power Sources*, **499**, 229901 (2021).
3. W. Li, I. Demir, D. Cao, D. Jöst, F. Ringbeck, M. Junker, and D. U. Sauer, "Data-driven systematic parameter identification of an electrochemical model for lithium-ion batteries with artificial intelligence." *Energy Storage Materials*, **44**, 557 (2022).
4. N. A. Chaturvedi, R. Klein, J. Christensen, J. Ahmed, and A. Kojic, "Algorithms for advanced battery-management systems." *IEEE Control Systems*, **30**, 49 (2010).
5. L. D. Couto, R. Romagnoli, S. Park, D. Zhang, S. J. Moura, M. Kinnaert, and E. Garone, "Faster and healthier charging of lithium-ion batteries via constrained feedback control." *IEEE Transactions on Control Systems Technology*, **30**, 1990 (2022).
6. A. Allam and S. Onori, "On-line capacity estimation for lithium-ion battery cells via an electrochemical model-based adaptive interconnected observer." *IEEE Transactions on Control Systems Technology*, **29**, 1636 (2021).
7. M. D. Berliner, H. Zhao, S. Das, M. Forsuelo, B. Jiang, W. H Chueh, M. Z Bazant, and R. D Braatz, "Nonlinear identifiability analysis of the porous electrode theory model of lithium-ion batteries." *J. Electrochem. Soc.*, **168**, 090546 (2021).
8. Q. Lai, H. Jun Ahn, Y. J. Kim, Y. N. Kim, and X. Lin, "New data optimization framework for parameter estimation under uncertainties with application to lithium-ion battery." *Applied Energy*, **295**, 117034 (2021).
9. D. G. Cacuci, M. Ionescu-Bujor, and I. M. Navon, *Sensitivity and Uncertainty Analysis* (Chapman & Hall/CRC Press, Boca Raton) (2003).
10. Q. Lai, S. Jangra, H. J. Ahn, G. Kim, W. T. Joe, and X. Lin, "Analytical sensitivity analysis for battery electrochemical parameters." *2019 American Control Conference (ACC)*890 (2019).
11. Q. Lai, S. Jangra, H. J. Ahn, G. Kim, W. T. Joe, and X. Lin, "Analytical derivation and analysis of parameter sensitivity for battery electrochemical dynamics." *J. Power Sources*, **472**, 228 (2020).
12. N. Jin, D. L. Danilov, P. M. J. Van den Hof, and M. C. F. Donkers, "Parameter estimation of an electrochemistry-based lithium-ion battery model using a two-step procedure and a parameter sensitivity analysis." *Int. J. Energy Research*, **42**, 2417 (2018).
13. A. J. van Rensburg, G. van Schoor, and P. A. van Vuuren, "Stepwise global sensitivity analysis of a physics-based battery model using the Morris method and Monte Carlo experiments." *J. Energy Storage*, **25**, 100875 (2019).
14. X. Lai, Z. Meng, S. Wang, X. Han, L. Zhou, T. Sun, X. Li, X. Wang, Y. Ma, and Y. Zheng, "Global parametric sensitivity analysis of equivalent circuit model based on Sobol method for lithium-ion batteries in electric vehicles." *J. Cleaner Production*, **294**, 126246 (2021).
15. T. M. Cover and J. A. Thomas, *Elements of Information Theory* (Wiley, Hoboken, NJ) 2nd Eda ed.392 (2006).
16. A. P. Schmidt, M. Bitzer, Á. W Imre, and L. Guzzella, "Experiment-driven electrochemical modeling and systematic parameterization for a lithium-ion battery cell." *J. Power Sources*, **195**, 5071 (2010).
17. A. Sharma and H. K. Fathy, "Fisher identifiability analysis for a periodically-excited equivalent-circuit lithium-ion battery model." *2014 American Control Conference (ACC), IEEE*, Portland, OR, USA274 (2014).
18. H. Cramér, *Mathematical Methods of Statistics (PMS-9)* (Princeton University Press) (1999).
19. X. Lin and A. G. Stefanopoulou, "Analytic bound on accuracy of battery state and parameter estimation." *J. Electrochem. Soc.*, **162**, A1879 (2015).
20. X. Lin, "On the analytic accuracy of battery SOC, capacity and resistance estimation." *2016 American Control Conference (ACC), IEEE*, Boston, MA, USA4006 (2016).
21. X. Lin, "Analytic analysis of the data-dependent estimation accuracy of battery equivalent circuit dynamics." *IEEE Control Systems Letters*, **1**, 304 (2017).
22. V. V. Fedorov, *Theory of Optimal Experiments* (Academic Press, Inc., New York, NY)27 (1972).
23. S. Park, D. Kato, Z. Gima, R. Klein, and S. Moura, "Optimal experimental design for parameterization of an electrochemical lithium-ion battery model." *J. Electrochem. Soc.*, **165**, A1309 (2018).
24. Q. Lai, H. J. Ahn, G. Kim, W. T. Joe, and X. Lin, "Optimization of current excitation for identification of battery electrochemical parameters based on analytic sensitivity expression." *2020 American Control Conference (ACC)*346 (2020).
25. Y. Wu, Q. Xue, J. Shen, Z. Lei, Z. Chen, and Y. Liu, "State of health estimation for lithium-ion batteries based on healthy features and long short-term memory." *IEEE Access*, **8**, 28533 (2020).
26. N. Zhou, X. Zhao, B. Han, P. Li, Z. Wang, and J. Fan, "A novel quick and robust capacity estimation method for Li-ion battery cell combining information energy and singular value decomposition." *J. Energy Storage*, **50**, 104263 (2022).
27. V. Ramadesigan, K. Chen, N. A. Burns, V. Boovaragavan, R. D. Braatz, and V. R. Subramanian, "Parameter estimation and capacity fade analysis of lithium-ion batteries using reformulated models." *J. Electrochem. Soc.*, **158**, A1048 (2011).
28. J. Vazquez-Arenas, L. E. Gimenez, M. Fowler, T. Han, and S.-K. Chen, "A rapid estimation and sensitivity analysis of parameters describing the behavior of commercial Li-ion batteries including thermal analysis." *Energy Conversion and Management*, **87**, 472 (2014).
29. P. P. Mishra, M. Garg, S. Mendoza, J. Liu, C. D. Rahn, and H. K. Fathy, "How does model reduction affect lithium-ion battery state of charge estimation errors? Theory and experiments." *J. Electrochem. Soc.*, **164**, A237 (2017).
30. X. Lin, "Theoretical analysis of battery SOC estimation errors under sensor bias and variance." *IEEE Trans. Ind. Electron.*, **65**, 7138 (2018).
31. X. Lin, A. Stefanopoulou, P. Laskowsky, J. Freudenberg, Y. Li, and R. D. Anderson, "State of charge estimation error due to parameter mismatch in a generalized explicit lithium ion battery model." *Dynamic Systems and Control Conference***1**, 393 (2011).
32. J Fogelquist and X Lin, "Uncertainty-aware data selection framework for parameter estimation with application to Li-ion battery." *2022 American Control Conference (ACC), IEEE*384 (2022).
33. J Fogelquist and X Lin, "Data selection framework for battery state of health related parameter estimation under system uncertainties." *eTransportation*, under review.
34. M. Doyle, T. F. Fuller, and J. Newman, "Modeling of galvanostatic charge and discharge of the lithium/polymer/insertion cell." *J. Electrochem. Soc.*, **140**, 1526 (1993).
35. E. Prada, D. Di Domenico, Y. Creff, J. Bernard, V. Sauvant-Moynot, and F. Huet, "Simplified electrochemical and thermal model of LiFePO $_4$ -Graphite Li-ion batteries for fast charge applications." *J. Electrochem. Soc.*, **159**, A1508 (2012).
36. S. J. Moura, F. B. Argomedo, R. Klein, A. Mirtabatabaei, and M. Krstic, "Battery state estimation for a single particle model with electrolyte dynamics." *IEEE Transactions on Control Systems Technology*, **25**, 453 (2017).
37. A. P. Schmidt, M. Bitzer, A. W. Imre, and L. Guzzella, "Model-based distinction and quantification of capacity loss and rate capability fade in Li-ion batteries." *J. Power Sources*, **195**, 7634 (2010).
38. G. K. Prasad and C. D. Rahn, "Model based identification of aging parameters in lithium ion batteries." *J. Power Sources*, **232**, 79 (2013).
39. X. Lin, "A data selection strategy for real-time estimation of battery parameters." *2018 American Control Conference (ACC)*2276 (2018).
40. J. Liu, S. Mendoza, and H. K. Fathy, "Total least squares state of charge estimation for lithium-ion batteries: an efficient moving horizon estimation approach." *IFAC-PapersOnLine*, **50**, 14489 (2017).
41. J. C. Forman, S. J. Moura, J. L. Stein, and H. K. Fathy, "Genetic identification and Fisher identifiability analysis of the Doyle-Fuller-Newman model from experimental cycling of a LiFePO $_4$ cell." *J. Power Sources*, **210**, 263 (2012).
42. M. A. Rahman, S. Anwar, and A. Izadian, "Electrochemical model parameter identification of a lithium-ion battery using particle swarm optimization method." *J. Power Sources*, **307**, 86 (2016).
43. J. Beck and K. Arnold, *Parameter Estimation in Engineering and Science* (Wiley) (1977).
44. C. R. Birkl, M. R. Roberts, E. McTurk, P. G. Bruce, and D. A. Howey, "Degradation diagnostics for lithium ion cells." *J. Power Sources*, **341**, 373 (2017).
45. X. Han, L. Lu, Y. Zheng, X. Feng, Z. Li, J. Li, and M. Ouyang, "A review on the key issues of the lithium ion battery degradation among the whole life cycle." *eTransportation*, **1**, 100005 (2019).
46. S. A. Channagiri, S. C. Nagpure, S. S. Babu, G. J. Noble, and R. T. Hart, "Porosity and phase fraction evolution with aging in lithium iron phosphate battery cathodes." *J. Power Sources*, **243**, 750 (2013).

47. G. Dong and J. Wei, "A physics-based aging model for lithium-ion battery with coupled chemical/mechanical degradation mechanisms." *Electrochimica Acta*, **395**, 139133 (2021).
48. P. Ramadass, B. Haran, R. White, and B. N. Popov, "Mathematical modeling of the capacity fade of Li-ion cells." *J. Power Sources*, **123**, 230 (2003).
49. R. Fang, C. Miao, Y. Nie, D. Wang, W. Xiao, M. Xu, and C. Wang, "Degradation mechanism and performance enhancement strategies of $LiNi_x Co_y Al_{1-x-y} O_2$ ($x \geqslant 0.8$) cathodes for rechargeable lithium-ion batteries: a review." *Ionics*, **26**, 3199 (2020).
50. D. Di Domenico, A. Stefanopoulou, and G. Fiengo, "Lithium-ion battery state of charge and critical surface charge estimation using an electrochemical model-based extended Kalman filter." *J. Dyn. Syst. Meas. Control*, **132**, 061302 (2010).
51. G. Fan, K. Pan, and M. Canova, "A comparison of model order reduction techniques for electrochemical characterization of lithium-ion batteries." *2015 54th IEEE Conference on Decision and Control (CDC), IEEE*, Osaka, 3922 (2015).
52. J. C. Forman, S. Bashash, J. L. Stein, and H. K. Fathy, "Reduction of an electrochemistry-based Li-ion battery model via quasi-linearization and Padé approximation." *J. Electrochem. Soc.*, **158**, A93 (2011).
53. N. T. Tran, M. Vilathgamuwa, T. Farrell, S. S. Choi, Y. Li, and J. Teague, "A Padé approximate model of lithium ion batteries." *J. Electrochem. Soc.*, **165**, A1409 (2018).
54. C.-H. Chen, F. Brosa Planella, K. O'Regan, D. Gastol, W. D. Widanage, and E. Kendrick, "Development of experimental techniques for parameterization of multi-scale lithium-ion battery models." *J. Electrochem. Soc.*, **167**, 080534 (2020).